J|A|C|S ARTICLES

Published on Web 07/15/2010

$XeOF_3^-$, an Example of an AX_3YE_2 Valence Shell Electron Pair Repulsion Arrangement; Syntheses and Structural Characterizations of $[M][XeOF_3]$ ($M = Cs, N(CH_3)_4$)

David S. Brock, Hélène P. A. Mercier, and Gary J. Schrobilgen*

Department of Chemistry, McMaster University, Hamilton, Ontario L8S 4M1, Canada

Received May 1, 2010; E-mail: schrobil@mcmaster.ca

Abstract: The $XeOF_3^-$ anion has been synthesized as its Cs^+ and $N(CH_3)_4^+$ salts and structurally characterized in the solid state by low-temperature Raman spectroscopy and quantum-chemical calculations. Vibrational frequency assignments for $[Cs][XeOF_3]$ and $[N(CH_3)_4][XeOF_3]$ were aided by ^{18}O enrichment. The calculated anion geometry is based on a square planar AX_3YE_2 valence-shell electron-pair repulsion arrangement with the longest Xe−F bond trans to the oxygen atom. The F−Xe−F angle is bent away from the oxygen atom to accommodate the greater spatial requirement of the oxygen double bond domain. The experimental vibrational frequencies and trends in their isotopic shifts are reproduced by the calculated gas-phase frequencies at several levels of theory. The $XeOF_3^-$ anion of the Cs^+ salt is fluorine-bridged in the solid state, whereas the anion of the $N(CH_3)_4^+$ salt has been shown to best approximate the gas-phase anion. Although $[Cs][XeOF_3]$ and $[N(CH_3)_4][XeOF_3]$ are shock-sensitive explosives, the decomposition pathways for the anions have been inferred from their decomposition products at 20 °C. The latter consist of XeF_2, $[Cs][XeO_2F_3]$, and $[N(CH_3)_4][F]$. Enthalpies and Gibbs free energies of reaction obtained from Born−Fajans−Haber thermochemical cycles support the proposed decomposition pathways and show that both disproportionation to XeF_2, $[Cs][XeO_2F_3]$, and CsF and reduction to XeF_2, CsF, and O_2 are favorable for $[Cs][XeOF_3]$, while only reduction to XeF_2 accompanied by $[N(CH_3)_4][F]$ and O_2 formation are favorable for $[N(CH_3)_4][XeOF_3]$. In all cases, the decomposition pathways are dominated by the lattice enthalpies of the products.

Introduction

Although the xenon(IV) fluoride species XeF_3^+,[1−3] XeF_4,[4−6] and XeF_5^- [7] have been well characterized spectroscopically and by single-crystal X-ray diffraction, the absence of a facile synthetic route to high-purity $XeOF_2$ had prevented extensive exploration of its fluoride ion donor−acceptor properties. The recent synthesis of pure $XeOF_2$[8] has provided an opportunity to extend the oxide fluoride chemistry of Xe(IV) and to study the fluoride ion acceptor properties of $XeOF_2$ with the view to synthesize and characterize salts of the $XeOF_3^-$ anion.

A prior publication has reported the synthesis of $[Cs][XeOF_3]$ and its characterization by low-temperature Raman spectroscopy.[9] The synthesis (eqs 1 and 2) utilized anhydrous HF (aHF) as the solvent medium, which was complicated by the fact that both F^- and $XeOF_2$[8] form HF solvates. Removal of HF under dynamic vacuum at −78 °C produced a mixture of $XeOF_2$ and $[Cs][F(HF)_n]$.

$$CsF + mHF \xrightarrow[-78\ °C]{HF} [Cs][F(HF)_m] \quad (1)$$

$$[Cs][F(HF)_m] + XeOF_2 \xrightarrow[0\ °C]{\text{dynamic vac}} [Cs][XeOF_3] + mHF \quad (2)$$

Slow warming of the product mixture to room temperature under dynamic vacuum resulted in further removal of HF. The authors concluded that, upon solvent removal, the reaction proceeded to the formation of $[Cs][XeOF_3]$, along with traces of $[Cs][XeO_2F_3]$; the latter was attributed to a disproportionation (eq 3).[9] The present work will show that a mixture of XeF_2, $XeOF_2$, $[Cs][XeF_5]$, and $[Cs][XeO_3F]$ was actually formed in the earlier reported work and that the $XeOF_3^-$ anion has eluded synthesis until the present work.

$$2[Cs][XeOF_3] \xrightarrow[0\ °C]{HF} [Cs][XeO_2F_3] + XeF_2 + CsF \quad (3)$$

(1) Gillespie, R. J.; Schrobilgen, G. J.; Landa, B. *J. Chem. Soc. D* **1971**, 1543–1544.
(2) Boldrini, P.; Gillespie, R. J.; Ireland, P. R.; Schrobilgen, G. J. *Inorg. Chem.* **1974**, *13*, 1690–1694.
(3) McKee, D. E.; Zalkin, A.; Bartlett, N. *Inorg. Chem.* **1973**, *12*, 1713–1717.
(4) Claassen, H. H.; Chernick, C. L.; Malm, J. G. *J. Am. Chem. Soc.* **1963**, *85*, 1927–1928.
(5) Schumacher, G. A.; Schrobilgen, G. J. *Inorg. Chem.* **1984**, *23*, 2923–2929.
(6) Levy, H. A.; Burns, J. H.; Agron, P. A. *Science* **1963**, *139*, 1208–1209.
(7) Christe, K. O.; Curtis, E. C.; Dixon, D. A.; Mercier, H. P.; Sanders, J. C. P.; Schrobilgen, G. J. *J. Am. Chem. Soc.* **1991**, *113*, 3351–3361.
(8) Brock, D. S.; Bilir, V.; Mercier, H. P. A.; Schrobilgen, G. J. *J. Am. Chem. Soc.* **2007**, *129*, 3598–3611.
(9) Gillespie, R. J.; Schrobilgen, G. J. *J. Chem. Soc., Chem. Commun.* **1977**, 595–597.

The $XeOF_3^-$ anion is of special interest because, to the best of the authors' knowledge, it represents the only example of an AX_3YE_2 valence-shell electron-pair repulsion (VSEPR)[10] arrangement in which the valence electron lone-pair domains and a double-bond domain occupy positions where they are approximately 90° to one another (Structure I).

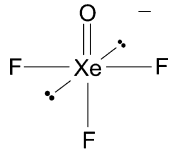

I

The present paper details the syntheses of the Cs^+ and $N(CH_3)_4^+$ salts of the $XeOF_3^-$ anion and their characterization by Raman spectroscopy. Quantum-chemical calculations and ^{18}O enrichment have been employed to assign the Raman spectra of the $Xe^{16/18}OF_3^-$ anion and to aid in the assessment of its chemical bonding.

Results and Discussion

Syntheses of $[M][XeOF_3]$ ($M = N(CH_4)$, Cs). (a) $[M][XeOF_3]$ in CH_3CN Solvent. Reactions and the purities of all products were routinely monitored by recording the low-temperature Raman spectra (−150 °C) of the natural abundance and ^{18}O-enriched (98.6 atom %) $XeOF_3^-$ salts.

The $XeOF_3^-$ anion was obtained as the $N(CH_3)_4^+$ and Cs^+ salts by the low-temperature reaction of $XeOF_2$ with $[N(CH_3)_4][F](CsF)$ in dry CH_3CN solvent according to eq 4, where $M = N(CH_3)_4$, Cs.

$$XeOF_2 + [M][F] \xrightarrow[-45\ °C]{CH_3CN} [M][XeOF_3] \quad (4)$$

Tetramethylammonium fluoride or CsF was added in ca. 3−5% excess to circumvent possible $XeOF_2$ contamination of the product. The $[N(CH_3)_4][XeOF_3]$ salt precipitated from solution as a very pale yellow, amorphous powder and was isolated by removal of the solvent under dynamic vacuum at −45 to −42 °C over a period of several hours. The synthesis of $[Cs][XeOF_3]$ was complicated by the low solubilities of CsF and $[Cs][XeOF_3]$ in CH_3CN solvent. Upon warming, $XeOF_2$ reacted in varying degrees with CsF, forming insoluble $[Cs][XeOF_3]$ in admixture with unreacted CsF. Unreacted $XeOF_2$, which imparted a yellow color to the supernatant, remained in solution and was removed by use of a cannula as previously described.[8] The residual solvent was removed under dynamic vacuum at −45 to −42 °C over a period of several hours, leaving behind a pale yellow powder. Reaction of [M][F] with $XeOF_2$ in 2:1 molar ratios yielded only $[M][XeOF_3]$ and did not result in the formation of $[M]_2[XeOF_4]$. Conversely, reaction of the fluoride salts with $XeOF_2$ in 1:2 molar ratios did not result in the formation of $F_2OXe{---}F{---}XeOF_2^-$ salts, yielding only $[M][XeOF_3]$ and unreacted $XeOF_2$.

(b) Attempts To Replicate the Prior Synthesis of "$[Cs][XeOF_3]$" in aHF. A 1:1 molar ratio of CsF and $XeOF_2$ was prepared in aHF and dried under dynamic vacuum at −78 °C. The product was shown by Raman spectroscopy to be $XeOF_2 \cdot nHF$, but presumably also contained $[Cs][F(HF)_m]$. With further pumping, vigorous mixing, and slow warming to −10 °C to remove additional bound HF, the original pale yellow color of the sample intensified. The Raman spectrum of the resulting solid revealed a mixture of $XeOF_2$ and $[Cs][XeOF_3]$ (and presumably $[Cs][F(HF)_n]$, where $n \ll m$).

The previously reported synthesis of "$[Cs][XeOF_3]$", which was carried out at 0 °C,[9] closely resembles the present synthesis, which was carried out at −10 °C. However, the Raman spectra of their respective products are significantly different. The Raman spectrum of the previously reported product mixture[9] has now been reassigned to XeF_2, $XeOF_2$, $[Cs][XeF_5]$, and $[Cs][XeO_3F]$ (Table S1 in the Supporting Information). It is likely that none of the reactions leading to the latter products involve $[Cs][XeOF_3]$ as an intermediate because none of its vibrational bands were observed in the Raman spectra of the product mixtures based on the present Raman assignments for $[Cs][XeOF_3]$ (cf. Tables 1 and S1). The neutral molecules, $XeOF_2$ and XeF_2, likely form upon removal of HF from $XeOF_2 \cdot nHF$ (eq 5),[8] followed by either xenon(IV) reduction to xenon(II) (eq 6)[8] or disproportionation (eq 7).[8,9] The previous report also noted that the reaction of XeF_4 and H_2O in HF solvent at −60 °C, which was used to synthesize $XeOF_2$, was incomplete and therefore contained unreacted XeF_4 and H_2O.[9] Xenon tetrafluoride, which has been shown to react with CsF to form $[Cs][XeF_5]$,[7] presumably reacts with $[Cs][F(HF)_n]$ according to eq 8.[11] Water and $[Cs][F(HF)_n]$ would form $[Cs][XeO_3F]$ by either hydrolysis of XeO_2F_2 (eq 9),[12] followed by fluoride ion addition[13] (eq 10), or by fluoride ion addition to XeO_2F_2[14] (eq 11), followed by hydrolysis (eq 12). Equations 11 and 12 represent the most likely route to $[Cs][XeO_3F]$ because $[Cs][XeO_2F_3]$ was often observed in the Raman spectra of product mixtures but XeO_3 was not.[9] The hydrolysis of XeF_5^- in the presence of unreacted H_2O, which competes with Xe(VI) species in eqs 9 and 12, does not occur and is consistent with the higher oxophilicities of Xe(VI) species (see Reactivities of $XeOF_3^-$ Salts).

$$XeOF_2 \cdot nHF \rightarrow XeOF_2 + nHF\uparrow \quad (5)$$

$$XeOF_2 \rightarrow XeF_2 + \tfrac{1}{2}O_2 \quad (6)$$

$$XeOF_2 \rightarrow \tfrac{1}{2}XeF_2 + \tfrac{1}{2}XeO_2F_2 \quad (7)$$

$$XeF_4 + [Cs][F(HF)_n] \rightarrow [Cs][XeF_5] + nHF\uparrow \quad (8)$$

$$XeO_2F_2 + H_2O \rightarrow XeO_3 + 2HF \quad (9)$$

$$XeO_3 + [Cs][F(HF)_n] \rightarrow [Cs][XeO_3F] + nHF\uparrow \quad (10)$$

$$XeO_2F_2 + [Cs][F(HF)_n] \rightarrow [Cs][XeO_2F_3] + nHF\uparrow \quad (11)$$

$$[Cs][XeO_2F_3] + H_2O \rightarrow [Cs][XeO_3F] + 2HF \quad (12)$$

(c) An Alternative Synthesis of $[Cs][XeOF_3]$. High-purity $[Cs][XeOF_3]$ was obtained when HF solvent was removed from a stoichiometric mixture of CsF and $XeOF_2$ at −78 °C, followed by warming the reaction mixture to −45 °C under dynamic vacuum. Solid $XeOF_2$, which forms an insoluble HF solvate,[8] appeared to liquify and became intense yellow in color prior to formation of a dry yellow powder under dynamic vacuum. The Raman spectrum of this intermediate mixture showed only $XeOF_2$. It is presumed that $[Cs][F(HF)_m]$ was also present but could not be observed in the Raman spectrum because the bands were too broad and weak. Extraction of residual HF with an

(10) Gillespie, R. J.; Hargittai, I. *The VSEPR Model of Molecular Geometry*; Allyn and Bacon: Boston, MA, 1991; pp 154−155.

aliquot of CH_3CN at −20 °C resulted in high-purity $[Cs][XeOF_3]$. The present method avoids decomposition arising from higher reaction temperatures and heterogeneous reaction conditions that result from the synthetic procedure outlined in the section above by using CH_3CN to partially or completely solubilize $XeOF_2$ and CsF.

Hydrolytic and Thermal Stabilities of $[M][XeOF_3]$ (M = $N(CH_4)$, Cs). Dry $[N(CH_3)_4][XeOF_3]$ is shock sensitive at low temperatures but does not exhibit shock sensitivity under CH_3CN upon standing at room temperature for 10 min. Dry $[N(CH_3)_4][XeOF_3]$ is kinetically stable at −78 °C for indefinite periods of time but begins to slowly decompose upon warming from 0 to 10 °C. The low-temperature (−150 °C) Raman spectra of samples briefly warmed to 25 °C and then quenched at −150 °C show the growth of the $\nu_s(XeF_2)$ band of XeF_2 at 498 cm^{-1} [15] and the $\nu(CH_3)$ bands of $[N(CH_3)_4][F]$ at 2957 and 3038 cm^{-1}.[16−18] The $[Cs][XeOF_3]$ salt is also stable at −78 °C for indefinite periods of time but slowly decomposes at room temperature to XeF_2, $XeO_2F_3^-$, O_2, and CsF. Although $[Cs][XeOF_3]$ appears to be less shock sensitive than the $N(CH_3)_4^+$ salt, detonations have occurred when attempting to transfer the finely powdered salt in a drybox.

Two decomposition pathways have been inferred for $XeOF_3^-$ on the basis of these observations. The major decomposition pathway is through reduction to Xe(II) (eq 13), and the minor decomposition pathway is through disproportionation (eq 14) to Xe(II) and Xe(VI) (see Thermochemistry).

$$[M][XeOF_3] \rightarrow XeF_2 + \tfrac{1}{2}O_2 + [M][F] \quad (13)$$

$$[M][XeOF_3] \rightarrow \tfrac{1}{2}XeF_2 + \tfrac{1}{2}[M][XeO_2F_3] + \tfrac{1}{2}[M][F] \quad (14)$$

While $[Cs][XeOF_3]$ and $[N(CH_3)_4][XeOF_3]$ can be obtained as pure salts when exact stoichiometric ratios of XeF_4 and H_2O are used for the synthesis of $XeOF_2$, both salts hydrolyze when H_2O is used in excess. Characterization of the hydrolysis products by Raman spectroscopy showed several bands in the frequency range 720−785 cm^{-1}. The bands appearing between 720 and 765 cm^{-1} correspond to the ν(XeO) regions for $XeOF_2$,[8] $F_2OXeNCCH_3$,[8] $XeOF_2 \cdot nHF$,[8] and $XeOF_3^-$, while the bands appearing between 745 and 785 cm^{-1} correspond to the $\nu_s(XeO_3)$ regions for XeO_3F^-[13] and XeO_3.[19] The findings indicate that the decomposition pathway resulting from hydrolysis involves disproportionation to Xe(VI)-containing species that likely occurs according to eqs 15 and 16. Although the exact nature of the decomposition product(s) could not be established, it is likely to be a compound(s) having the general formulation(s) $[Cs]_x[(XeO_3)_yF_x(XeOF_2)_z]$.

$$XeOF_3^- + H_2O \xrightarrow[-45\ ^\circ C]{CH_3CN} [XeO_2F^-] + 2HF \quad (15)$$

$$[XeO_2F^-] \xrightarrow[-45\ ^\circ C]{CH_3CN} \tfrac{1}{2}XeO_3F^- + \tfrac{1}{2}Xe + \tfrac{1}{2}O_2 + \tfrac{1}{2}F^- \quad (16)$$

Reactivities of $XeOF_3^-$ Salts. The insolubilities and/or reactivities of the $N(CH_3)_4^+$ and Cs^+ salts in CH_3CN, SO_2, SO_2ClF, HF, $XeOF_4$, ONF, and O_2NF have prevented crystal growth and NMR characterization.

Attempts to dissolve $[N(CH_3)_4][XeOF_3]$ in SO_2 at −78 °C resulted in sample detonation, and it is proposed that $XeOF_3^-$ oxidizes SO_2 to SO_3 according to eq 17.

$$[N(CH_3)_4][XeOF_3] + SO_2 \xrightarrow[-78\ ^\circ C]{neat} XeF_2 + SO_3 + [N(CH_3)_4][F] \quad (17)$$

An attempt to dissolve $[Cs][XeOF_3]$ in $XeOF_4$ at ca. 20 °C resulted in oxygen/fluorine metathesis to give XeF_4, XeO_2F_2, and $[Cs][F(XeOF_4)_m]$[20] according to eq 18.

$$[Cs][XeOF_3] + (m+1)XeOF_4 \xrightarrow[20\ ^\circ C]{neat} XeF_4 + XeO_2F_2 + [Cs][F(XeOF_4)_m] \quad (18)$$

The syntheses of the NO^+ and NO_2^+ salts of $XeOF_3^-$ were attempted. Contact of ONF with $XeOF_2$ at −78 °C resulted in an explosion in which $XeOF_2$ likely oxidizes ONF to O_2NF (eq 19).

$$ONF + XeOF_2 \xrightarrow[-78\ ^\circ C]{neat} O_2NF + XeF_2 \quad (19)$$

The white residue that remained and coated the fractured FEP reaction vessel had an odor reminiscent of XeF_2. Addition of O_2NF to $XeOF_2$ at −78 °C resulted in an immediate color change from yellow to white upon contact with liquid O_2NF. The Raman spectrum of the product mixture showed modes corresponding to XeF_4, N_2O_5 (the spectrum corresponded to the ionic solid-state formulation $[NO_2][NO_3]$[21]), and XeF_5^- anion bands. The Raman spectrum (Table S2 in the Supporting Information) indicates that $XeOF_2$ transfers oxygen to O_2NF to give XeF_4 and N_2O_5 (eq 20) and a subsequent reaction of O_2NF with XeF_4 gives the XeF_5^- anion (eq 21).

$$2O_2NF + XeOF_2 \xrightarrow[-78\ ^\circ C]{neat} XeF_4 + N_2O_5 \quad (20)$$

$$XeF_4 + O_2NF \xrightarrow[-78\ ^\circ C]{neat} [NO_2][XeF_5] \quad (21)$$

Raman Spectroscopy. The low-temperature Raman spectra of $[N(CH_3)_4][Xe^{16/18}OF_3]$ and $[Cs][Xe^{16/18}OF_3]$ are shown in Figures 1 and 2, respectively. The observed and calculated frequencies and their assignments are listed in Tables 1 and 2 and in Tables S3 and S4 of the Supporting Information. In the absence of a crystal structure, the energy-minimized geometry

(11) To confirm this assumption, an intimate mixture of XeF_4 and $[Cs][F(HF)_n]$ was created by dissolving an equimolar mixture of XeF_4 and CsF in aHF. The solution was quenched at −196 °C, and HF was removed under dynamic vacuum at −78 °C. Warming this XeF_4/$[Cs][F(HF)_n]$ mixture to 0 °C under dynamic vacuum yielded a small amount of $[Cs][XeF_5]$ in admixture with XeF_4, which was verified by Raman spectroscopy at −150 °C.

(12) Huston, J. L. *J. Phys. Chem.* **1967**, *71*, 3339–3341.
(13) LaBonville, P.; Ferraro, J. R.; Spittler, T. M. *J. Chem. Phys.* **1971**, *55*, 631–640.
(14) Christe, K. O.; Wilson, W. W. *Inorg. Chem.* **1988**, *27*, 3763–3768.
(15) Agron, P. A.; Begun, G. M.; Levy, H. A.; Mason, A. A.; Jones, C. G.; Smith, D. F. *Science* **1963**, *139*, 842–844.
(16) Berg, R. W. *Spectrochim. Acta* **1978**, *34A*, 655–659.
(17) Kabisch, G.; Klose, M. *J. Raman Spectrosc.* **1978**, *7*, 311–315.
(18) Kabisch, G. *J. Raman Spectrosc.* **1980**, *9*, 279–285.
(19) Smith, D. F. *J. Am. Chem. Soc.* **1963**, *85*, 816–817.

(20) There is precedent for polynuclear anions of the type $F(XeOF_4)_m^-$ with the synthesis and structural characterization of the $(XeOF_4)_3F^-$ anion as its Cs^+ salt: Holloway, J. H.; Kaučič, V.; Martin-Rovet, D.; Russell, D. R.; Schrobilgen, G. J.; Selig, H. *Inorg. Chem.* **1985**, *24*, 678–683.

(21) Wilson, W. W.; Christe, K. O *Inorg. Chem.* **1987**, *26*, 1631–1633.

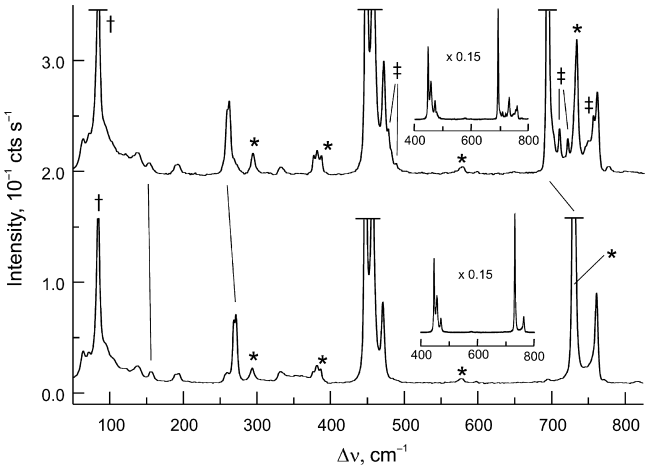

Figure 1. Raman spectra of natural abundance (lower trace) and 97.8% ^{18}O-enriched (upper trace) $[N(CH_3)_4][XeOF_3]$ recorded at −150 °C using 1064-nm excitation. Symbols denote FEP sample tube lines (*), instrumental artifact (†), and minor hydrolysis product(s) (‡).

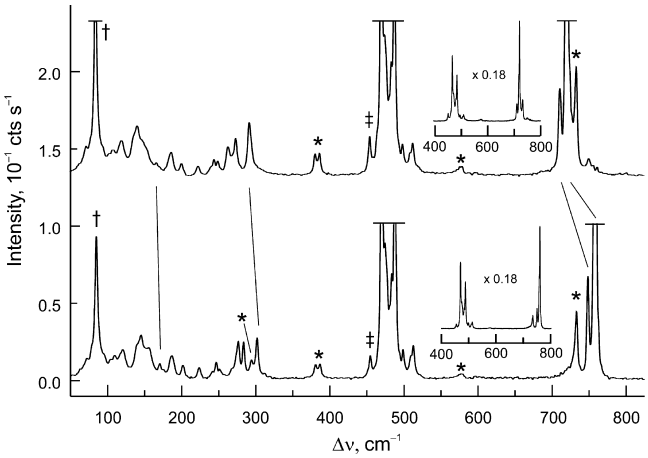

Figure 2. Raman spectra of natural abundance (lower trace) and 97.8% ^{18}O-enriched (upper trace) $Cs[XeOF_3]$ recorded at −150 °C using 1064-nm excitation. Symbols denote FEP sample tube lines (*), instrumental artifact (†), and minor hydrolysis product(s) (‡).

of the $XeOF_3^-$ anion was calculated at several levels of theory (Tables 2, S3, and S4) using the aug-cc-pVDZ(-PP) and aug-cc-pVTZ(-PP) basis sets. The calculated vibrational frequencies, intensities, and $^{16/18}$O-isotopic shifts were used to assign the Raman spectra of $Xe^{16}OF_3^-$ and $Xe^{18}OF_3^-$ in their Cs^+ and $N(CH_3)_4^+$ salts. Regardless of the level of theory or basis set used, the frequency, intensity, and isotopic shift trends are similar and consistent. The frequency ranges cited in the ensuing discussion refer to isotopic shifts and are the values obtained for the entire range of theory levels, showing good agreement with experiment regardless of the level of theory used. The experimental and calculated vibrational frequencies for monomeric $XeOF_2$ and their assignments (Table S5 in the Supporting Information) have been previously discussed[8] and were also used to aid in the vibrational assignments of $XeOF_3^-$.

The $Xe^{16/18}OF_3^-$ anion possesses C_{2v} symmetry, which results in nine fundamental vibrational modes that span the irreducible representations $4A_1 + 3B_1 + 2B_2$ (the xz-plane is the molecular plane and the Xe−O bond lies along the z-axis) which are both Raman and infrared active.

(a) $[N(CH_3)_4][XeOF_3]$. The frequencies associated with the $N(CH_3)_4^+$ cation have been assigned on the basis of comparisons

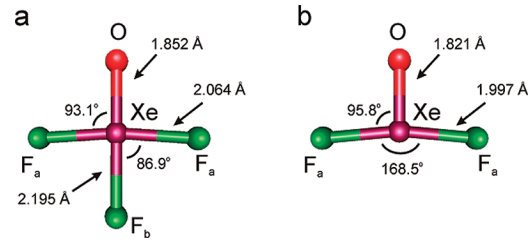

Figure 3. Calculated geometries [B3LYP/aug-cc-pVTZ(-PP)] for (a) $XeOF_3^-$ and (b) $XeOF_2$.

with the previous literature.[16−18] The $XeOF_3^-$ anion of $[N(CH_3)_4][XeOF_3]$ is in overall good agreement with the calculated gas-phase anion. As predicted from the calculated frequencies and Raman intensities, the highest frequency and most intense $XeOF_3^-$ band occurs at 730.1 cm^{-1} and is assigned to ν(XeO). This mode displays a large low-frequency shift (−36.1 cm^{-1}) upon ^{18}O substitution that is in very good agreement with the calculated values (−33.5 to −42.8 cm^{-1}). The asymmetric $\nu_{as}(XeF_{2a})$ mode is expected to be weak to very weak in the Raman spectrum and was not observed. The bands at 457.3/471.3 and 447.6 cm^{-1} are of medium intensity and are assigned to the in-plane stretching modes $\nu_s(XeF_{2a}) + \nu(XeF_b)$ and $\nu_s(XeF_{2a}) - \nu(XeF_b)$, respectively. Their frequencies are essentially unshifted upon ^{18}O-enrichment, which is expected for modes that do not involve oxygen atom displacements. The band at 332.0 cm^{-1} is assigned to the out-of-plane deformation mode, $\delta(XeOF_3)$, and appears as a weak band, in agreement with the calculated Raman intensity, and shows no ^{18}O dependence although the calculations predict a small isotopic shift (−2.8 to −3.8 cm^{-1}). The split band at 268.7, 271.5 cm^{-1} is sensitive to isotopic substitution and is assigned to the in-plane deformation mode, $\rho_{rock}(XeOF_{2a})$. The experimental ^{18}O isotopic shift for this mode, −9.3, −9.6 cm^{-1}, is in good agreement with the calculated values (−7.5 to −9.3 cm^{-1}). The weak bands at 189.5, 193.9 cm^{-1} are insensitive to ^{18}O substitution and are assigned to the in-plane XeF_2 bending mode. The band at 156.5 cm^{-1} is assigned to the out-of-plane $\delta(XeOF_b) - \delta(XeF_{2a})$ mode and shows a small isotopic shift (−3.6 cm^{-1}), in agreement with the calculated values (−1.4 to −1.9 cm^{-1}). The lowest frequency band at 137.8 cm^{-1} is also weak, displaying no isotopic shift, in accordance with the small calculated values (−0.1 to −1.2 cm^{-1}), and is assigned to the in-plane deformation mode, $\rho_{rock}(OXeF_{2a}) + \delta(F_bXeF_a)$.

The low-frequency shifts of the stretching modes relative to their counterparts in $XeOF_2$ and $F_2OXeNCCH_3$[8] are consistent with anion formation and increased Xe−O and Xe−F bond polarities in the anion. These low-frequency shifts are reproduced by the quantum-chemical calculations.

(b) $[Cs][XeOF_3]$. The Raman spectrum of the Cs^+ salt is very similar to that of the $N(CH_3)_4^+$ salt, although the bands are shifted to higher frequencies, which likely results from significant cation−anion contacts. The bands that are the most affected are shifted by as much as 30 cm^{-1} and correspond to modes that involve oxygen atom displacements, i.e., ν(XeO) and $\rho_{rock}(XeOF_{2a})$, indicating that the Cs^+ cation likely coordinates most strongly to the oxygen atom. These findings are in agreement with the NBO analysis (see Computational Results), which assigns most of the negative charge to the oxygen atom. Weak bands between 223 and 276 cm^{-1} in the Cs^+ salt are absent in the $N(CH_3)_4^+$ salt. These bands are in the appropriate region and are of appropriate intensity for stretching modes associated with fluorine bridges,[20] suggesting an oligomeric or

Table 1. Experimental Raman Frequencies[a] and Intensities[b] for $XeOF_3^-$ in $Cs[XeOF_3]$ and $[N(CH_3)_4][XeOF_3]$

Cs^+ salt[c,d,e]			$N(CH_3)_4^+$ salt[c,d,f]			assgnts[h]
$Xe^{16}OF_3^-$	$Xe^{18}OF_3^-$	Δν	$Xe^{16}OF_3^-$	$Xe^{18}OF_3^-$[g]	Δν	(C_{2v}) symmetry
759.6(100)	721.4(100)	–38.2				
757.2 sh	719.0 sh	–38.2	730.1(100)	694.0(100)	–36.1	ν(XeO)
748.9(20)	711.3(17)	–37.6				
512.8(6)	512.7(6)	–0.1				
509.7(4)	508.9(4)	–0.8	n.o.	n.o.		$\nu_{as}(XeF_{2a})$
498.9(5)	498.9(6)	0.0				
487.7(46)	487.6(45)	–0.1	471.3(12)	472.0(16)	0.7	$\nu_s(XeF_{2a}) + \nu(XeF_b)$
483.8(20)	483.7(22)	–0.1	457.3(31)	457.4(34)	–0.1	
474.5(26)	474.5(28)	0.0	447.6(63)	447.5(66)	–0.1	$\nu_s(XeF_{2a}) - \nu(XeF_b)$
470.2(65)	470.2(65)	0.0				
n.o.	n.o.		332.0(2)	332.4(1)	0.4	$\delta(XeOF_3)$ o.o.p.
301.6(8)	292.0(8)	–9.6	271.5(10)	261.9(11)	–9.6	$\rho_{rock}(OXeF_{2a})$ i.p.
283.2(7)	273.6(6)	–9.6	268.7(9)	259.4(9)	–9.3	
276.4(7)	263.2(6)	–13.2				
250.9(2)	249.6(3)	–1.3				
246.6(3)	244.5(3)	–2.1				fluorine bridge modes
241.4(1)	239.7 sh	–1.7				
223.4(2)	223.0(2)	–0.4				
201.2(3)	200.3(2)	–0.9	193.9(1)	193.1(1)	–0.8	$\delta(XeF_{2a})$ i.p.
186.8(4)	186.4(5)	–0.4	189.5(1)	189.0(1)	–0.5	
170.2(3)	166.7(2)	–3.5	156.5(2)	152.9(1)	–3.6	$[\delta(OXeF_b) - \delta(XeF_{2a})]$ o.o.p.
154.9(6)	147.5sh	–7.4				
144.9(8)	140.5(10)	–4.4	137.8(2)	137.7(3)	–0.1	$[\rho_{rock}(OXeF_{2a}) + \delta(F_bXeF_a)]$ i.p.
138.8 sh	134.9 sh	–3.9				
119.8(6)	119.1(7)	–0.7				lattice modes
108.7(4)	108.7(5)	0.0				

[a] Frequencies are given in cm^{-1}. [b] Values in parentheses denote relative Raman intensities. [c] Raman spectra were recorded in FEP sample tubes at −150 °C using 1064-nm excitation. [d] The abbreviations denote shoulder (sh) and not observed (n.o.). [e] Weak bands at 454.7(4) and 763.1(sh) in the ^{16}O spectrum and at 454.5(7) and 724.8(sh) in the ^{18}O spectrum are attributed to a hydrolysis product(s). [f] The $N(CH_3)_4^+$ cation modes were observed at $\nu_8(E)$, 377(2); $\nu_{19}(T_2)$, 460(2); $\nu_3(A_1)$, 761(13); $\nu_{18}(T_2)$, 951(10); $\nu_7(E)$, 1176(2), 1187(1); $\nu_{17}(T_2)$, 1287(1); $\nu_{16}(T_2)$, 1405(2), 1408(2); $\nu_2(A_1)$, $\nu_6(E)$, 1462(12), 1479(1), 1487(10); $\nu(CH_3)$ and combination bands, 2800(2), 2881sh, 2908(3), 2938(3), 2957(12), 2978sh, 2999sh, 3038(18) cm^{-1}. [g] Weak bands at 756.2(8), 749.4(5), 744.7(3), 721.3(5) 710.0(6), 702.1sh, 488.8(1), 481.9(3), and 478.2(6) in the ^{18}O spectrum are attributed to hydrolysis product(s). The band at 472.0(16) also partially overlaps with a hydrolysis product band. [h] The abbreviations denote symmetric (s), asymmetric (as), stretch (ν), bend (δ), rock (ρ_{rock}), in-plane bend (i.p.), and out-of-plane bend (o.o.p.). The in-plane and out-of-plane mode descriptions are relative to the $XeOF_{2a}F_b$ plane, i.e., the anion lies in the *xz*-plane with the Xe−O bond collinear with the *z*-axis (see Figure 3).

chain structure for $[Cs][XeOF_3]$. Such long contacts most likely result in coupling between $XeOF_3^-$ units which not only would account for the splittings of the vibrational bands but also may result in symmetry reduction and observation of the $\nu_{as}(XeF_{2a})$ stretching mode at 498.9, 509.7, and 512.8 cm^{-1} which was not observed in the $N(CH_3)_4^+$ salt.

Computational Results. Because a crystal structure for a $XeOF_3^-$ salt is not available, a series of quantum-chemical calculations at different levels of theory with different basis sets were carried out (Table 2 and 3 and Tables S3, S4, and S6 in the Supporting Information). All calculations resulted in stationary points with all frequencies real. The calculations established that trends in the vibrational frequencies persisted at all levels of theory and for all basis sets used. The calculated frequencies and their trends were then compared with the observed trends, allowing reliable assignments of the experimental Raman frequencies to be made. The parent compound, $XeOF_2$,[8] was used as a benchmark for the calculations (Table S5). Values for the aug-cc-pVTZ(-PP) basis set are reported along with those of the aug-cc-pVDZ(-PP) basis set. The latter are given in square brackets.

(a) Geometries. The geometry of the $XeOF_3^-$ anion optimized at C_{2v} symmetry, yielding a planar structure that is in accord with that predicted by the VSEPR model of molecular geometry[10] (see Raman Spectroscopy, above). As noted for $XeOF_2$,[8] the use of a larger basis set tends to give shorter bond lengths and smaller $O-Xe-F_a$ bond angles. With the exception of the BP86 method, where the bonds are significantly elongated, all bond lengths fall within relatively narrow ranges (Xe−O, 1.821−1.859 [1.854−1.890] Å; $Xe-F_a$, 2.032−2.064 [2.061−2.096] Å; $Xe-F_b$, 2.129−2.195 [2.131−2.205] Å). As predicted by the VSEPR rules,[10] the $Xe-F_a$ bonds are shorter than the $Xe-F_b$ bond. In general, all bond angles are also within a narrow range, with the exception of the MP2 value, which gives a larger $O-Xe-F_a$ angle than other levels of theory. The fluorine atoms, F_a, are displaced away from the oxygen atom, with an $O-Xe-F_a$ angle of 92.8−93.7 [93.1−94.2]° and an F_a-Xe-F_a angle of 172.5−174.4 [171.7−173.9]°. When compared with $XeOF_2$, the net −1 charge of $XeOF_3^-$ results in longer $Xe-F_a$ and Xe−O bonds and a F_a-Xe-F_a angle that is closer to linearity than in $XeOF_2$ (164.8−170.8°).

(b) Natural Bond Orbital (NBO) Analyses. The NBO[22−25] analyses were carried out for all optimized gas-phase geometries

(22) Reed, A. E.; Weinstock, R. B.; Weinhold, F. *J. Chem. Phys.* **1985**, *83*, 735–746.
(23) Reed, A. E.; Curtiss, L. A.; Weinhold, F. *Chem. Rev.* **1998**, *88*, 899–926.
(24) Glendening, E. D.; Reed, A. E.; Carpenter, J. E.; Weinhold, F. *NBO Version 3.1*; Gaussian Inc.: Pittsburgh, PA, 1990.

Table 2. Selected Calculated Vibrational Frequencies[a] and Infrared and Raman Intensities[b] for the $Xe^{16/18}OF_3^-$ Anion[c]

MP2	PBE1PBE	B3LYP	assignment[d]
		$Xe^{16}OF_3^-$	
867.9 (25) [241]	771.2 (59) [160]	729.6 (62) [152]	ν(XeO)
493.6 (<1) [283]	491.2 (<0.1) [340]	467.3 (<0.1) [319]	$\nu_{as}(XeF_{2a})$
460.7 (27) [152]	460.5 (34) [54]	432.7 (37) [66]	$\nu_s(XeF_{2a}) + \nu(XeF_b)$
379.2 (20) [34]	372.3 (10) [131]	356.9 (13) [106]	$\nu_s(XeF_{2a}) - \nu(XeF_b)$
286.8 (<1) [54]	269.4 (<1) [48]	256.3 (<1) [47]	$\delta(XeOF_3)$ o.o.p.
250.6 (4) [<1]	259.9 (3) [<1]	246.9 (4) [<1]	$\rho_{rock}(OXeF_{2a})$ i.p.
171.2 (<1) [2]	183.6 (<1) [1]	177.2 (<1) [2]	$\delta(XeF_{2a})$ i.p.
132.6 (<1) [<0.1]	136.6 (<1) [<1]	127.5 (<1) [<1]	$\delta(OXeF_b) - \delta(XeF_{2a})$ o.o.p.
150.5 (<1) [2]	115.6 (1) [1]	119.8 (1) [1]	$\rho_{rock}(OXeF_{2a}) + \delta(F_bXeF_a)$ i.p.
		$Xe^{18}OF_3^-$	
825.1 (22) [224]	733.4 (53) [51]	694.0 (54) [145]	ν(XeO)
494.8 (<1) [284]	492.5 (<0.1) [341]	468.5 (<0.1) [319]	$\nu_{as}(XeF_{2a})$
461.0 (27) [151]	460.6 (10) [129]	432.8 (38) [65]	$\nu_s(XeF_{2a}) + \nu(XeF_b)$
379.3 (20) [33]	372.3 (10) [129]	356.8 (13) [104]	$\nu_s(XeF_{2a}) - \nu(XeF_b)$
283.0 (<1) [52]	266.6 (<1) [46]	253.4 (<1) [46]	$\delta(XeOF_3)$ o.o.p.
242.6 (4) [<1]	250.8 (3) [<1]	238.4 (4) [<1]	$\rho_{rock}(OXeF_{2a})$ i.p.
171.2 (<1) [2]	183.6 (<1) [1]	177.2 (<1) [2]	$\delta(XeF_{2a})$ i.p.
131.1 (<1) [0]	134.7 (<1) [<1]	125.8 (<1) [<1]	$\delta(OXeF_b) - \delta(XeF_{2a})$ o.o.p.
149.3 (<1) [2]	115.0 (1) [1]	119.2 (1) [1]	$\rho_{rock}(OXeF_{2a}) + \delta(F_bXeF_a)$ i.p.

[a] Frequencies are given in cm^{-1}. [b] Values in parentheses denote calculated Raman intensities ($Å^4\ u^{-1}$). Values in square brackets denote calculated infrared intensities (km mol^{-1}). [c] The aug-cc-pVTZ(-PP) basis set was used. [d] The abbreviations denote symmetric (s), asymmetric (as), stretch (ν), bend (δ), rock (ρ_{rock}), in-plane bend (i.p.), and out-of-plane bend (o.o.p.). The in-plane and out-of-plane mode descriptions are relative to the $XeOF_{2a}F_b$ plane (see Figure 3 and footnote *h* of Table 1.

Table 3. Calculated Geometrical Parameters for the $XeOF_3^-$ Anion[a]

	MP2	SVWN5	BP86	PBE1PBE	B3LYP	B3PW91	MPW1PW91
				Bond Lengths (Å)			
$Xe-F_a$	2.060	2.064	2.106	2.032	2.064	2.048	2.034
Xe−O	1.821	1.859	1.881	1.830	1.852	1.840	1.831
$Xe-F_b$	2.129	2.143	2.188	2.173	2.195	2.178	2.175
				Bond Angles (deg)			
$O-Xe-F_a$	94.8	93.7	93.7	92.9	93.1	93.0	92.8
F_a-Xe-F_b	85.2	86.3	86.3	87.1	86.9	87.0	87.2
F_a-Xe-F_a	170.3	172.6	172.5	174.3	173.9	173.9	174.4

[a] The aug-cc-pVTZ(-PP) basis set was used.

of $XeOF_3^-$ and $XeOF_2$ for comparison and are summarized in Tables S7 and S8 of the Supporting Information. The results at all levels of theory are similar, and therefore only the MP2 values are referred to in the ensuing discussion.

The natural population analysis (NPA) charges of 2.11 and 2.13 for Xe in $XeOF_3^-$ and $XeOF_2$, respectively, show that the charge on xenon remains essentially unchanged upon anion formation and is approximately half of the formal charge that is given by a purely ionic model, indicating that the anion bonds are polar covalent. Upon formation of $XeOF_3^-$ from $XeOF_2$, the net negative charge of the anion is dispersed among the more electronegative atoms, yielding natural charges for O (−1.038), F_a (−0.762 each), and F_b (−0.654) that are higher than the corresponding values in $XeOF_2$. The charge on O is about half of its formal oxidation number, while the F charges are approximately two-thirds of their formal oxidation number, indicating that the bonds are more ionic in the anion than in neutral $XeOF_2$. Among the plausible valence bond Structures I−IV and VI−IX for $XeOF_3^-$ (see Scheme S1 in the Supporting Information), the calculated charges are best represented by Structure V, which is an average of Structures II−IV, with a somewhat larger contribution from Structure II. The Xe−O/$Xe-F_a$ and Xe−O/$Xe-F_b$ bond order ratios, 3.43 and 2.65, respectively, and Xe/O/F_a/F_b valencies (1.509/0.703/0.213/0.257) are in overall agreement with a composite of these resonance contributions.

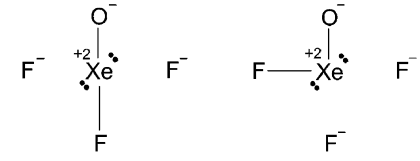

II III

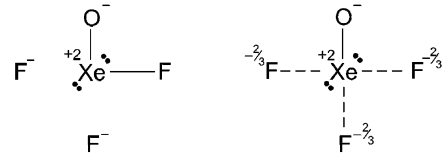

IV V

Upon anion formation, donation of electron density by the fluoride ion into the xenon valence shell results in substantial decreases in the Xe−O and Xe−F bond orders and Xe valency and increases in the O and F valencies relative to those of $XeOF_2$. Thus, the Xe−O and Xe−F bonds are somewhat more ionic in $XeOF_3^-$ when compared with those in $XeOF_2$.

(25) Glendening, E. D.; Badenhoop, J. K.; Reed, A. E.; Carpenter, J. E.; Bohmann, C. M.; Morales, C. M.; Weinhold, F. *NBO Version 5.0*; Theoretical Chemistry Institute, University of Wisconsin: Madison, WI, 2001.

Table 4. Estimated Volumes, Lattice Enthalpies, and Entropies for $N(CH_3)_4^+$ and Cs^+ Salts of F^-, $XeOF_3^-$, and $XeO_2F_3^-$

Salt	V_m (nm^3)	ΔH°_L (kJ mol^{-1}) [a]	S° (J mol^{-1} K^{-1}) [b]
$[N(CH_3)_4][F]$	0.1460 [c]	554.4	213.5
$[N(CH_3)_4][XeOF_3]$	0.2168 [d]	499.3	309.9
	0.2192 [e]	497.9	313.1
$[N(CH_3)_4][XeO_2F_3]$ [e]	0.2302 [f]	491.6	328.0
[Cs][F]	0.0573 [c]	717.3	92.9
[Cs][XeOF$_3$]	0.1282 [d]	574.1	189.3
	0.1305 [e]	571.3	192.5
$[Cs][XeO_2F_3]$ [e]	0.1415 [f]	559.0	207.4

[a] The lattice enthalpies (ΔH°_L) were calculated as described in ref 28. [b] The standard entropies were calculated as described in ref 30. [c] The formula unit volumes, V_m, for $[N(CH_3)_4][F]$ and CsF were obtained from their crystallographic unit cells at −163 (ref 32) and 25 °C (ref 33), respectively. [d] The values for V_m[M][XeOF$_3$] were estimated by $V_m(F_2OXeNCCH_3$; 0.1324 nm^3, ref 8) − $V_m(CH_3CN$; 0.0616 nm^3, ref 34) + V_m([M][F]). [e] The V_m values for [M][XeOF$_3$] were estimated by V_m([M][F]) + [$V_m(XeF_2$; 0.0622 nm^3, ref 35) + $V_m(XeO_2F_2$; 0.0842 nm^3, ref 36)]/2. [f] The V_m values for [M][XeO_2F_3] were estimated by V_m([M][F]) + $V_m(XeO_2F_2$; 0.0842 nm^3, ref 36).

Table 5. Values of ΔH°, ΔS°, and ΔG° Calculated for the Decomposition Reactions of [M][XeOF$_3$] (X = $N(CH_3)_4$, Cs)[a]

	ΔH° (kJ mol^{-1})		ΔS° (J mol^{-1} K^{-1})		ΔG° (kJ mol^{-1})	
$[N(CH_3)_4][XeOF_3]_{(s)} \rightarrow XeF_{2(s)} + {}^1/_2O_{2(g)} + [N(CH_3)_4][F]_{(s)}$	−58.2	−59.6	121.3	118.1	−94.3	−94.7
$[N(CH_3)_4][XeOF_3]_{(s)} \rightarrow {}^1/_2XeF_{2(s)} +$ ${}^1/_2[N(CH_3)_4][XeO_2F_3]_{(s)} + {}^1/_2[N(CH_3)_4][F]_{(s)}$	4.9	3.5	18.4	15.2	−0.6	−1.1
$[Cs][XeOF_3]_{(s)} \rightarrow XeF_{2(s)} + {}^1/_2O_{2(g)} + [Cs][F]_{(s)}$	−146.3	−145.1	121.3	118.1	−182.4	−184.3
$[Cs][XeOF_3]_{(s)} \rightarrow {}^1/_2XeF_{2(s)} + {}^1/_2[Cs][XeO_2F_3]_{(s)} + {}^1/_2[Cs][F]_{(s)}$	−35.6	−38.4	18.4	15.2	−41.1	−42.9

[a] The first column under the headings ΔH°, ΔS°, and ΔG° was obtained from V_m([M][XeOF$_3$]) = $V_m(F_2OXeNCCH_3)$ − $V_m(CH_3CN)$ + V_m([M][F]), whereas the second column was obtained from V_m([M][XeOF$_3$]) = V_m([M][F]) + [$V_m(XeF_2)$ + $V_m(XeO_2F_2)$]/2.

Thermochemistry. To account for the different decomposition routes for $[N(CH_3)_4][XeOF_3]$ and [Cs][XeOF$_3$], quantum-chemical calculations and established semiempirical methods[26−30] were used in conjunction with known thermodynamic quantities to estimate ΔH°, ΔS°, and ΔG° for eqs 13 and 14.

The standard enthalpies for the decomposition reactions were determined by analyzing their Born−Fajans−Haber cycles. The enthalpy changes for the gas-phase reduction (eq 22) and disproportionation (eq 23) reactions were calculated using the MP2 method.

$$XeOF_3^-{}_{(g)} \rightarrow XeF_{2(g)} + ½O_{2(g)} + F^-{}_{(g)} \qquad (22)$$

$$\Delta H^\circ = +52.6\text{kJ mol mol}^{-1} \qquad \text{MP2/aug-cc-pVTZ(-PP)}$$

$$XeOF_3^-{}_{(g)} \rightarrow ½XeF_{2(g)} + ½XeO_2F_3^-{}_{(g)} + ½F^-{}_{(g)} \qquad (23)$$

$$\Delta H^\circ = +56.3\text{kJ mol mol}^{-1} \qquad \text{MP2/aug-cc-pVTZ(-PP)}$$

The experimental value for the enthalpy of sublimation (ΔH_{sub}) for XeF_2 (55.71 kJ mol^{-1}) was used.[31] The lattice enthalpies of [M][F], [M][XeOF$_3$], and [M][XeO_2F_3] (Table 4) were estimated by use of the volume-based method of Bartlett et al.,[26,27] as generalized by Jenkins et al.[28,29] in eq 24, where R is the gas constant (8.314 J K^{-1} mol^{-1}), I is the ionicity of the salt, and the constants α, β, and p depend on the nature of the salt.

$$\Delta H^\circ_L = 2I\left(\frac{\alpha}{\sqrt[3]{V_m}} + \beta\right) + pRT \qquad (24)$$

For the salts under investigation, which are singly charged and nonlinear, the following values were used: $I = 1$, $\alpha = 117.3$ nm kJ mol^{-1}, $\beta = 51.9$ kJ mol^{-1}, and $p = 2$. In this formalism, ΔH°_L is the lattice enthalpy, defined as the energy required to break the crystal lattice, and therefore has a positive value. This approach is generally accurate to ∼4% for salts with $\Delta H^\circ_L <$ 5000 kJ mol^{-1},[29] and is particularly useful because the formula unit volume (V_m) of an unknown salt can be estimated with reasonable accuracy using several methods.[29,37] The net enthalpies of decomposition (eqs 25 and 26) calculated for the reductions (ΔH°_{red}) and disproportionations (ΔH°_{dis}) of [M][XeOF$_3$] (M = $N(CH_3)_4$, Cs) are summarized in Table 5.

$$\Delta H^\circ_{red} = \Delta H^\circ_L([M][XeOF_3]) - \Delta H^\circ(\text{eq 22}) - \Delta H^\circ_L([M][F]) - \Delta H^\circ(\text{sub } XeF_2) \qquad (25)$$

$$\Delta H^\circ_{dis} = \Delta H^\circ_L([M][XeOF_3]) - \Delta H^\circ(\text{eq 23}) - ½\Delta H^\circ_L([M][F]) - ½\Delta H^\circ_L([M][XeO_2F_3]) - \Delta H^\circ(\text{sub } XeF_2) \qquad (26)$$

A method for estimating the absolute standard entropy of a salt from its unit volume has been reported by Jenkins and Glasser (eq 27), where $k = 1360$ J K^{-1} mol^{-1} (nm^{-3} formula unit^{-1}) and $c = 15$ J K^{-1} mol^{-1}.[30]

$$S^\circ = kV_m + c \qquad (27)$$

Entropies for the [M][F], [M][XeOF$_3$], and [M][XeO_2F_3] salts under consideration are provided in Table 4. When coupled with

(26) Bartlett, N.; Yeh, S.; Kourtakis, K.; Mallouk, T. *J. Fluorine Chem.* **1984**, *26*, 97–116.
(27) Shen, C.; Hagiwara, R.; Mallouk, T.; Bartlett, N. In *Inorganic Fluorine Chemistry, Toward the 21st Century*; Thrasher, J. S., Strauss, S. H., Eds.; ACS Symposium Series *555*; American Chemical Society: Washington, DC, 1994; Chapter 2, pp 26−39.
(28) Jenkins, H. D. B.; Tudela, D.; Glasser, L. *Inorg. Chem.* **2002**, *41*, 2364–2367.
(29) Jenkins, H. D. B.; Roobottom, H. K.; Passmore, J.; Glasser, L. *Inorg. Chem.* **1999**, *38*, 3609–3620.
(30) Jenkins, H. D. B.; Glasser, L. *Inorg. Chem.* **2003**, *42*, 8702–8708.
(31) Osborne, D. W.; Flotow, H. E.; Malm, J. G. *J. Chem. Phys.* **1972**, *57*, 4670–4675.

the experimental standard entropies of $O_{2(g)}$ (206 J mol^{-1} K^{-1})[38] and $XeF_{2(s)}$ (115.09 J mol^{-1} K^{-1}),[31] this method allows $\Delta S°$ (eqs 28 and 29) and $\Delta G°$ (eq 30) to be calculated for the reactions of interest. The $\Delta S°$and $\Delta G°$ values obtained for these reactions are summarized in Table 5. Estimates of the unit volume of $XeOF_2$ using either the difference method ($V_m(F_2OXeNCCH_3) - V_m(CH_3CN) = 0.0708$ nm^3) or an average of the unit volumes of XeF_2 and XeO_2F_2 (0.0731 nm^3) differ by only 0.0023 nm^3 and lead to essentially the same $\Delta H°$ and $\Delta G°$ values.

$$\Delta S°_{red} = \tfrac{1}{2}S°(O_2) + S°([M][F]) + S°(XeF_2) - S°([M][XeOF_3]) \quad (28)$$

$$\Delta S° = \tfrac{1}{2}S°([M][F]) + \tfrac{1}{2}S°(XeF_2) + \tfrac{1}{2}S°([M][XeO_2F_3]) - S°([M][XeOF_3]) \quad (29)$$

$$\Delta G° = \Delta H° - T\Delta S° \quad (30)$$

Based on the aforementioned thermochemical calculations, both the gas-phase reduction and disproportionation pathways are endothermic, and the decompositions of the $[M][XeOF_3]$ salts are largely driven by lattice enthalpies. This is illustrated by the greater $\Delta H°$ and $\Delta G°$ values for the Cs^+ salt relative to those of the $N(CH_3)_4^+$ salt which result from the smaller size of Cs^+ and greater lattice enthalpies of CsF and $[Cs][XeO_2F_3]$.

The entropy term is also a major contributor in the reduction pathways because O_2 gas is evolved. The liberation of O_2 greatly increases the entropy of the reaction (119.7 J mol^{-1} K^{-1}) relative to the small entropy gain in the disproportionation pathways (16.8 J mol^{-1} K^{-1}). This results in the contribution of an additional -30.7 kJ mol^{-1} to the Gibbs free energies for the reduction pathways which, combined with the lattice enthalpies, renders the reduction pathways significantly more favorable than the disproportionation pathways for both salts.

Although the disproportionation of $[Cs][XeOF_3]$ is less favorable than reduction, the former is spontaneous. In contrast, $\Delta H°$ and $\Delta G°$ of the corresponding disproportionation reaction for $[N(CH_3)_4][XeOF_3]$ are close to zero. The larger size of the $N(CH_3)_4^+$ cation lowers the lattice enthalpies of $[N(CH_3)_4][F]$ and $[N(CH_3)_4][XeO_2F_3]$ such that they no longer overcome the gas-phase disproportionation enthalpy. The thermochemical calculations are in accordance with the observed decomposition products ($[N(CH_3)_4][F]$ and XeF_2) for $[N(CH_3)_4][XeOF_3]$, which can only decompose by the reduction pathway (eq 13). In contrast, $[Cs][XeOF_3]$, which can decompose by either the reduction (eq 13) or disproportionation (eq 14) pathway, resulted in the formation of predominantly XeF_2 and a small amount of $[Cs][XeO_2F_3]$.

Conclusion

The fluoride ion acceptor properties of $XeOF_2$ have been demonstrated by the high-yield syntheses of the endothermic salts, $[M][XeOF_3]$ ($M = N(CH_3)_4$, Cs), in high purity. Both salts are kinetically stable at -78 °C but slowly decompose at 10−25 °C. Their decomposition pathways, inferred from their decomposition products, are supported by their thermochemical cycles. The latter show that the proposed disproportionation and reduction pathways are mainly driven by lattice energy contributions, with entropy playing a significant role in the pathways that lead to reduction of Xe(IV) to Xe(II) and O_2 evolution. The thermochemical cycles also reveal that disproportionation of Xe(IV) to Xe(II) and Xe(VI) is favored for $[Cs][XeOF_3]$ but not for $[N(CH_3)_4][XeOF_3]$, in accordance with experiment.

Comparison of the solid-state vibrational spectrum of $[N(CH_3)_4][XeOF_3]$ with that of the calculated gas-phase $XeOF_3^-$ anion indicates little interaction between the anion and cation. The Raman spectra of the Cs^+ and $N(CH_3)_4^+$ salts of $XeOF_3^-$ also show that significant interactions occur between the Cs^+ cation and the oxygen atom of the $XeOF_3^-$ anion and that the anions interact with one another by means of fluorine bridges. The $XeOF_3^-$ anion is presently the only example of an AX_3YE_2 VSEPR arrangement known in which a double-bond domain subtends angles of ca. 90° with two valence electron lone-pair domains. Comparisons of the experimental frequencies of $[Cs][XeOF_3]$ with those previously reported for $[Cs][XeOF_3]$[9] reveal that the product obtained in an earlier study was a mixture of XeF_2, $XeOF_2$, $[Cs][XeF_5]$, and $[Cs][XeO_3F]$. Thus, the present work represents the first bona fide synthesis and characterization of the $XeOF_3^-$ anion.

Experimental Section

Caution. *The xenon(IV) oxide fluoride species, $XeOF_2$ and $[M][XeOF_3]$, are highly energetic, shock-sensitive materials and are only stable at the low temperatures described in the experimental procedures that outline their syntheses. Both $XeOF_2$ and $XeOF_3^-$ salts can detonate at low temperatures when mechanically or thermally shocked. Thus, adequate protective apparel and working behind adequate shielding are crucial for the safe manipulation of these materials. In the case of $XeOF_2$, detonations may occur upon freezing or further cooling of its CH_3CN solutions to −196 °C. It is strongly recommended that only small scale (<100 mg) syntheses of $XeOF_2$ and $XeOF_3^-$ salts be undertaken.*

Apparatus and Materials. (a) General. All manipulations involving air-sensitive materials were carried out under strictly anhydrous conditions as previously described.[39] Reaction vessels/Raman sample tubes were fabricated from $^1/_4$-in. o.d. FEP tubing and outfitted with Kel-F valves. All reaction vessels and sample tubes were rigorously dried under dynamic vacuum prior to passivation with 1 atm of F_2 gas.

Acetonitrile (Caledon, HPLC grade)[40] was purified by the literature method and transferred under static vacuum on a glass vacuum line. Sulfur dioxide was distilled into a thick-wall glass storage vessel containing P_4O_{10} and dried, with frequent agitation, for ca. 1 week prior to use. Dry SO_2 was then distilled directly from the storage vessel into the reaction vessel. Anhydrous HF (Harshaw Chemicals Co.) was purified by the literature method.[41] The high-purity syntheses and transfer methods for ONF and O_2NF are described in the Supporting Information. Xenon oxide difluoride[8] and $XeOF_4$[5] were prepared and purified according to the literature methods. Cesium fluoride (CsF, ICN-KCK Laboratories Inc., 99.9%) was dried by fusion in a platinum crucible, followed by immediate transfer of the melt to a drybox port which was immediately evacuated. Upon transferring to a nitrogen atmosphere

(32) Christe, K. O.; Wilson, W. W.; Wilson, R. D.; Bau, R.; Feng, J. *J. Am. Chem. Soc.* **1990**, *112*, 7619–7625.
(33) Cortona, P. *Phys. Rev. B: Condens. Matter* **1992**, *46*, 2008–2014.
(34) Torrie, B. H.; Powell, B. M. *Mol. Phys.* **1992**, *75*, 613–622.
(35) Lehmann, J. F. Ph.D. Thesis, McMaster University, Hamilton, ON, 2004.
(36) Peterson, S. W.; Willett, R. D.; Huston, J. L. *J. Chem. Phys.* **1973**, *59*, 453–459.
(37) Jenkins, H. D. B.; Glasser, L.; Klapötke, T. M.; Crawford, M.-J.; Bhasin, K. K.; Lee, J.; Schrobilgen, G. J.; Sunderlin, L. S.; Liebman, J. F. *Inorg. Chem.* **2004**, *43*, 6238–6248.
(38) Chase, M. W., Jr. *NIST JANAF Thermochemical Tables*; American Institute of Physics: New York, 1998.
(39) Casteel, W. J., Jr.; Dixon, D. A.; Mercier, H. P. A.; Schrobilgen, G. J. *Inorg. Chem.* **1996**, *35*, 4310–4322.
(40) Winfield, J. M. *J. Fluorine Chem.* **1984**, *25*, 91–98.
(41) Emara, A. A. A.; Schrobilgen, G. J. *Inorg. Chem.* **1992**, *31*, 1323–1332.

drybox, the sample was ground to a fine powder and stored in a PFA container inside the drybox until used. The naked fluoride ion source, $[N(CH_3)_4][F]$, was prepared according to the literature method[32] and was stored in an FEP tube in the drybox until used. Both H_2O (Caledon, HPLC grade) and $H_2{}^{18}O$ (MSD Isotopes, 97.8 atom % ^{18}O) were used without further purification to prepare 2.00 M $H_2{}^{16/18}O$ solutions in previously dried and purified CH_3CN[40] which were used in the synthesis of $XeOF_2$.[8] High-purity Ar (99.998%, Air Liquide) or N_2 (obtained from liquid N_2 boil-off and dried by passage through a column of dry 3 Å molecular sieves) gases were used for backfilling vessels.

(b) Syntheses of $[M][Xe^{16/18}OF_3]$ ($M = N(CH_3)_4$, Cs). In typical syntheses, a $^1/_4$-in. o.d. FEP reactor containing 0.306 mmol ($N(CH_3)_4^+$ salt) or 0.166 mmol (Cs^+ salt) of $Xe^{16/18}OF_2$ was cooled to −196 °C, and sufficient CH_3CN was condensed onto the walls of the reactor so that upon warming to −42 °C the solvent thawed, contacting, without detonation, and dissolving $Xe^{16/18}OF_2$. Alternatively, CH_3CN was syringed into the reactor in a manner identical to that used for the synthesis of $XeOF_2$.[8] Note: *In the event that the amount of CH_3CN added is insufficient to dissolve $XeOF_2$, the former method requires refreezing the sample at −196 °C, which often leads to sample detonation.*[8] The latter method is far less likely to lead to detonation and is preferred because CH_3CN is added at a higher temperature (−78 °C). The solution was quickly frozen at −78 °C and introduced into a drybox through a cold port, and 0.319 mmol of $[N(CH_3)_4][F]$ (0.171 mmol of CsF) was added while maintaining the reactor below −78 °C. The cold reactor was removed from the drybox and warmed to −42 °C, and the contents were thoroughly mixed, whereupon a pale yellow solid precipitated from solution. The solvent was removed under dynamic vacuum while maintaining the sample between −45 and −42 °C. The completeness of solvent removal was monitored by Raman spectroscopy and required several hours for the last traces of CH_3CN to be removed, resulting in pale yellow Cs^+ and $N(CH_3)_4^+$ salts.

(c) Attempted Syntheses of $[M'][XeOF_3]$ ($M' = NO, NO_2$). Approximately 0.2 mL of ONF or O_2NF was distilled into an evacuated sample tube containing $XeOF_2$ (43.3 mg for the ONF reaction; 49.7 mg for the O_2NF reaction) and frozen onto the vessel walls at −196 °C. The ONF or O_2NF was melted onto $XeOF_2$ at −78 °C. In the case of the ONF reaction, an immediate explosion ensued upon contact with $XeOF_2$. In the case of the O_2NF reaction, the solid immediately changed from yellow to white upon contact with liquid O_2NF.

(d) Reactivities of $[M][XeOF_3]$ with SO_2 and $XeOF_4$. In an effort to solubilize $[N(CH_3)_4][XeOF_3]$, ca. 0.2 mL of SO_2 was distilled into an evacuated sample tube containing 72.1 mg of $[N(CH_3)_4][XeOF_3]$ by freezing the condensate onto the walls of the reaction vessel at −196 °C. Upon warming the sample to −78 °C, contact of SO_2 vapor with the $[N(CH_3)_4][XeOF_3]$ resulted in an immediate explosion. In a second attempt, ca. 0.2 mL of $XeOF_4$ was frozen onto the upper walls of an evacuated 4-mm o.d. FEP sample tube containing 11.9 mg (0.0353 mmol) of $[Cs][XeOF_3]$ at −196 °C. The $XeOF_4$ was melted onto $[Cs][XeOF_3]$ at ca. 20 °C, and upon contact the solid rapidly turned from yellow to white. The $XeOF_4$ was removed under dynamic vacuum at ca. 20 °C, and a Raman spectrum of the white powder was recorded, revealing it to be a mixture XeF_4, XeO_2F_2, and $[Cs][F(XeOF_4)_m]$.[20]

Raman Spectroscopy. Raman spectra were recorded on a Bruker RFS 100 FT-Raman spectrometer at −150 °C using 1064 nm excitation, 300 mW laser power, and 1 cm^{-1} resolution as previously described.[42]

Computational Details. Geometries were fully optimized using MP2 and DFT (SVWN5, BP86, PBE1PBE, B3LYP, B3PW91, MPW1PW91) methods, and aug-cc-pVTZ and aug-cc-pVDZ basis sets were used for all atoms. Pseudopotentials were used for xenon (aug-cc-pVTZ-PP and aug-cc-pVDZ-PP), and their uses in combination with aug-cc-pVTZ and aug-cc-pVDZ are indicated by aug-cc-pVTZ(-PP) and aug-cc-pVDZ(-PP).[43] Fundamental vibrations were calculated, and NBO analyses[22−26] were performed for the optimized local minima at all levels. Quantum-chemical calculations were carried out using the program Gaussian 03[44] for geometry optimizations, vibrational frequencies, and their intensities. The program GaussView[45] was used to visualize the vibrational displacements that form the basis of the vibrational mode descriptions given in Table 2 and Tables S3−S5 of the Supporting Information.

Acknowledgment. We thank the Natural Sciences and Engineering Research Council of Canada for support in the form of a Discovery Grant (G.J.S.), the Ontario Graduate Scholarship in Science and Technology and the McMaster Internal Prestige "Ontario Graduate Fellowships" Programs for support (D.S.B.), and the computational resources provided by SHARCNet (Shared Hierarchical Academic Research Computing Network; www.sharcnet.ca).

Supporting Information Available: Reassigned Raman spectrum of products formerly attributed to $[Cs][XeOF_3]$ (Table S1); Raman spectrum of the products formed in the reaction of $XeOF_2$ with O_2NF (Table S2); calculated vibrational frequencies for $XeOF_3^-$ (Tables S3 and S4) and $XeOF_2$ (Table S5); calculated geometrical parameters for $XeOF_3^-$ (Tables S6); NBO valencies, bond orders, and NPA charges for $XeOF_3^-$ (Table S7) and $XeOF_2$ (Table S8); calculated geometrical parameters for $XeOF_2$ (Table S8); valence bond structures I−IV and VI−IX; detailed O_2NF and ONF syntheses; and complete ref 44. This material is available free of charge via the Internet at http://pubs.acs.org.

JA103730C

(42) Gerken, M.; Dixon, D. A.; Schrobilgen, G. J. *Inorg. Chem.* **2000**, *39*, 4244–4255.
(43) Basis sets were obtained from the Extensible Computational Chemistry Environment Basis set Database, version 2/25/04, as developed and distributed by the Molecular Science Computing Facility, Environmental and Molecular Science Laboratory, which is part of the Pacific Northwest Laboratory, P.O. Box 999, Richland, WA 99352.
(44) Frisch, M. J.; et al. *Gaussian 03*, revision D.01; Gaussian, Inc.: Wallingford, CT, 2004.
(45) *GaussView*, release 3.0; Gaussian Inc.: Pittsburgh, PA, 2003.